analytical chemistry

pubs.acs.org/ac
Article

Quantitative and Qualitative Analyses of Mass Spectra of OEL Materials by Artificial Neural Network and Interface Evaluation: Results from a VAMAS Interlaboratory Study

Satoka Aoyagi,* David J. H. Cant, Michael Dürr, Anya Eyres, Sarah Fearn, Ian S. Gilmore, Shin-ichi Iida, Reiko Ikeda, Kazutaka Ishikawa, Matija Lagator, Nicholas Lockyer, Philip Keller, Kazuhiro Matsuda, Yohei Murayama, Masayuki Okamoto, Benjamen P. Reed, Alexander G. Shard, Akio Takano, Gustavo F. Trindade, and Jean-Luc Vorng

Cite This: *Anal. Chem.* 2023, 95, 15078−15085

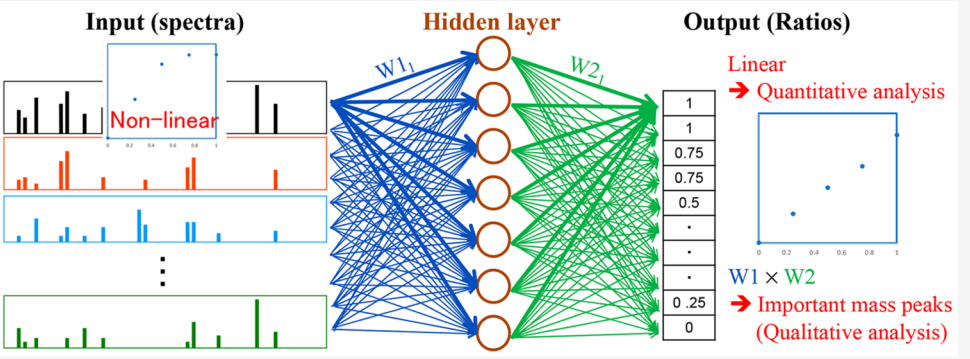

ABSTRACT: Quantitative analysis of binary mixtures of tris(2-phenylpyridinato)iridium(III) ($Ir(ppy)_3$) and tris(8-hydroxyquinolinato)aluminum (Alq_3) by using an artificial neural network (ANN) system to mass spectra was attempted based on the results of a VAMAS (Versailles Project on Advanced Materials and Standards) interlaboratory study (TW2 A31) to evaluate matrix-effect correction and to investigate interface determination. Monolayers of binary mixtures having different $Ir(ppy)_3$ ratios (0, 0.25, 0.50, 0.75, and 1.00), and the multilayers containing these mixtures and pure samples were measured using time-of-flight secondary ion mass spectrometry (ToF-SIMS) with different primary ion beams, OrbiSIMS (SIMS with both Orbitrap and ToF mass spectrometers), laser desorption ionization (LDI), desorption/ionization induced by neutral clusters (DINeC), and X-ray photoelectron spectroscopy (XPS). The mass spectra were analyzed using a simple ANN with one hidden layer. The $Ir(ppy)_3$ ratios of the unknown samples and the interfaces of the multilayers were predicted using the simple ANN system, even though the mass spectra of binary mixtures exhibited matrix effects. The $Ir(ppy)_3$ ratios at the interfaces indicated by the simple ANN were consistent with the XPS results and the ToF-SIMS depth profiles. The simple ANN system not only provided quantitative information on unknown samples, but also indicated important mass peaks related to each molecule in the samples without *a priori* information. The important mass peaks indicated by the simple ANN depended on the ionization process. The simple ANN results of the spectra sets obtained by a softer ionization method, such as LDI and DINeC, suggested large ions such as trimers. From the first step of the investigation to build an ANN model for evaluating mixture samples influenced by matrix effects, it was indicated that the simple ANN method is useful for obtaining candidate mass peaks for identification and for assuming mixture conditions that are helpful for further analysis.

Secondary ion mass spectrometry (SIMS) is useful for evaluating chemical species at surfaces and interfaces. However, quantitative analysis of multicomponent samples remains challenging because of matrix effects,[1−11] which cause ion-intensity changes irrespective of the concentration of the source material of the ion. To analyze inorganic material using SIMS, matrix effects are generally corrected by using relative sensitivity factors (RSF).[2,3] Various matrix-effect-correction methods for SIMS data of organic materials have been

Received: July 19, 2023
Accepted: September 5, 2023
Published: September 16, 2023

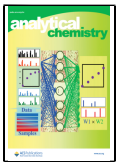

https://doi.org/10.1021/acs.analchem.3c03173
Anal. Chem. 2023, 95, 15078−15085

developed.[4−12] Although these methods are effective for the quantitative analysis of various organic binary mixtures,[12] it is still difficult to evaluate changes in the interface concentration. Moreover, matrix effects remain a major issue in quantitative analysis and mass imaging for other mass spectrometry techniques such as laser desorption ionization (LDI).[13]

Recently, soft ionization techniques using gas cluster ion beams (GCIBs), such as Ar clusters and water clusters, have been developed. In addition, 3D analysis of organic materials has become one of the most important applications of SIMS.[14,15] A previous VAMAS (Versailles Project on Advanced Materials and Standards) project on matrix effects reported that matrix effects tend to become more severe as the number of atoms in the primary ion cluster increases.[3] Therefore, the management of matrix effects is crucial for interpreting SIMS data using GCIB. Numerical analysis methods using artificial neural networks (ANNs) are useful for interpreting data based on nonlinear combinations, such as SIMS data containing matrix effects. Sparse autoencoders[16−19] composed of one middle layer show higher concentration dependence than that observed with conventional multivariate analysis methods, such as principal component analysis and multivariate curve resolution.[20,21] A simple ANN system with only one middle layer provides answers as well as processes to reach the answers regarding the relationship between the variables and the weights in ANNs.[19]

In this study, we prepared binary systems of organic electroluminescent (OEL) compounds tris(2-phenylpyridinato)iridium(III) ($Ir(ppy)_3$) and tris(8-hydroxyquinolinato)aluminum (Alq_3). Monolayers with different mixture ratios were used as standard samples for quantitative analysis. Multilayers of the mixtures and the pure layers of these OELs were evaluated using a simple ANN model trained with the standard samples. The OEL samples were measured using time-of-flight secondary ion mass spectrometry (ToF-SIMS), OrbiSIMS (SIMS with Orbitrap and ToF mass spectrometers), LDI, desorption/ionization induced by neutral clusters (DINeC), and X-ray photoelectron spectroscopy (XPS) through the VAMAS interlaboratory study TW2 A31. The LDI technique is generally not suited to molecular depth-profiling due to the requirement for matrix addition and due to the large sampling depth of the laser beam. However, LDI analysis is included here to provide additional information on ion formation from mixtures with different composition.

METHODS

OEL Sample Preparation. Two OEL materials, Ir(ppy)3 ($C_{33}H_{24}N_3Ir$, MW 655, density[22] 1.74 g/cm^3, Tokyo Chemical Industry Co. Ltd., Tokyo) and Alq_3 ($C_{27}H_{18}AlN_3O_3$, MW 459, density[23] 1.188 g/cm^3, Nippon Steel Chemical and Material Co. Ltd., Tokyo), were mixed in different ratios (mole fractions): 0.25:0.75, 0.5:0.5 and 0.75:0.25. Films containing $Ir(ppy)_3$ and Alq_3 were coevaporated onto cleaned Si wafer substrates using organic−inorganic vapor deposition equipment (C-E2L-1, Choshu Industry Co., Ltd., Yamaguchi, Japan). The Si substrates (1 cm × 1 cm) were first washed in isopropyl alcohol and ultrapure water using an ultrasonic wave cleaner and then cleaned with a UV ozone washer before producing films. The thicknesses of the films were 50 nm, and the distribution of the film thickness is less than 2%. The schematic of the samples was shown in Figure S1 in the Supporting Information.

Sample Measurement. *ToF-SIMS.* Each sample was measured using TOF-SIMS machines (ION-TOF GmbH, Munster, Germany, and ULVAC-PHI, Chigasaki, Japan) with pulsed Bi_3^{+2} as a primary ion source and Ar cluster ions as a sputtering ion source. The intensities reported herein are the steady-state intensities generated from Bi_3^{+2} primary ion impacts during an argon cluster depth-profile. ToF-SIMS measurement conditions are summarized in Table S1 of the Supporting Information.

ToF-SIMS with Water Clusters (J105). Positive ion spectra of each OEL sample were acquired with a J105 ToF-SIMS instrument (Ionoptika Ltd., U.K.) using a single charged H_2O cluster primary ion at 70 keV. In this work, the average water cluster size was 26,000 molecules. The system was described in detail elsewhere.[24] The mass range was m/z 0−1800, and the raster size was 500 μm × 500 μm.

OrbiSIMS. The instrument used for the analysis is an OrbiSIMS (Hybrid SIMS, IONTOF GmbH, Münster, Germany) equipped with a time-of-flight (ToF) mass analyzer and a Q Exactive HF Orbitrap mass analyzer (Thermo Fisher, Bremen, Germany). Further details are given in ref 25. For Orbitrap analysis, the mass-resolving power was set to 240000, with an injection time of 500 ms, and a mass range m/z 100−1500 was selected. A 5 keV Ar_{1400}^+ ion (26.4 pA, 20 μm spot size) was used for sputtering and analysis. The target potential was set at ±57.5 V. The pressure in the helium collision cell in the transfer optics was 0.042 bar using the low collisional cooling mode.[26] The floodgun and Argon gas flooding were off, as the sample did not require charge compensation. For the single layer samples, the beam was set to sputter an area of 313 μm × 313 μm, in which secondary ions were collected from the central 150 μm × 150 μm of the crater, apart from the 100% Alq_3 sample and the binary $Ir(ppy)_3$:Alq_3 (0.25:0.75) sample that had a beam sputter area of 280 μm × 280 μm in which secondary ions were collected from the central 200 μm × 200 μm of the crater. For the multilayer sample, the beam was set to sputter an area of 471 μm × 471 μm in which secondary ions were collected from the central 150 μm × 150 μm of the crater.

LDI-TOF. For obtaining LDI-TOF data, two sets of the OEL samples including the monolayer samples and the multilayer sample were separately measured with two ultrafleXtreme machines (Bruker) equipped with Smartbeam II laser (355 nm). Positive ion spectra were acquired in reflector mode. The mass range was m/z 0−2000. For one of the data sets, external standards, 2,5-DHB and C60, were added to the sample for the mass calibration and m/z 177 (2,5DHB+Na), 720 (C_{60}), and 840 (C_{70}) peaks were used.

DINeC. For the DINeC measurements, neutral SO_2 clusters were generated via supersonic expansion of a gas mixture of 3% SO_2 and 97% He through a pulsed nozzle operating at a pulse rate of 2 Hz with an effective opening time of 0.5 ms.[27,28] The gas pressure at the orifice of the nozzle was 15 bar. Under these conditions, clusters of a mean size of 10^3 to 10^4 SO_2 molecules with an energy density of E/n = 0.8 eV/molecule are obtained. Analysis of the desorbed ions was performed using a commercial ion trap mass spectrometer (amaZon speed, Bruker Daltonik GmbH, Bremen, Germany) that was equipped with a customer-built DINeC ion source.[28]

XPS. The multilayer sample was measured using XPS (Kratos AXIS Ultra) with monochromated Al Kalpha X-ray source Ir 4f, Al 2s and Si 2p were acquired in snapshot mode during the depth profile with pass energy 160 eV. The choice of core levels was made to avoid interferences and overlaps between photoelectron peaks. The sputter source was Ar_{1000}^+ at 5 keV with a beam current of 12 nA and a square raster area with side length 3 mm. Single-layer witness wafers were also measured by

https://doi.org/10.1021/acs.analchem.3c03173
Anal. Chem. 2023, 95, 15078−15085

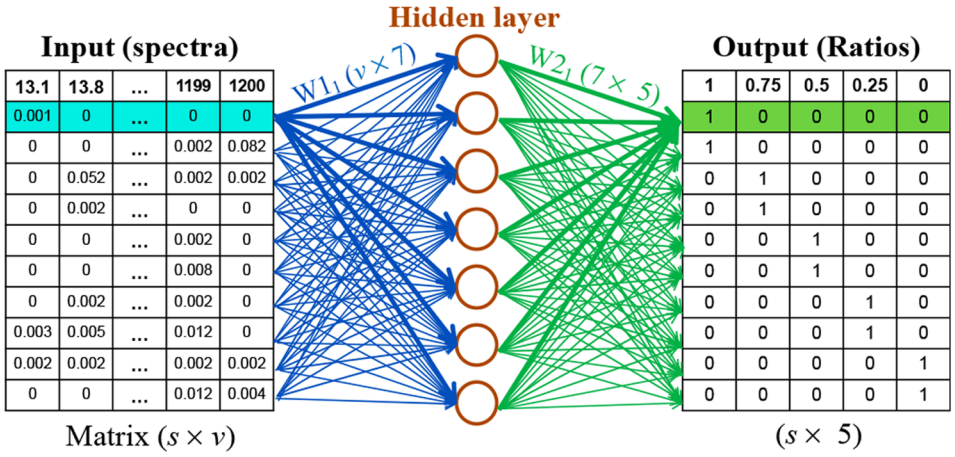

Figure 1. Concept of the simple ANN quantitative analysis system. Sizes of the hidden layer and labels (ratios) were 7 and 5, respectively. Numbers of the samples and the peaks (variables) are s and v, respectively. $W1_1$ and $W2_1$ were weights for the first sample highlighted in light blue.

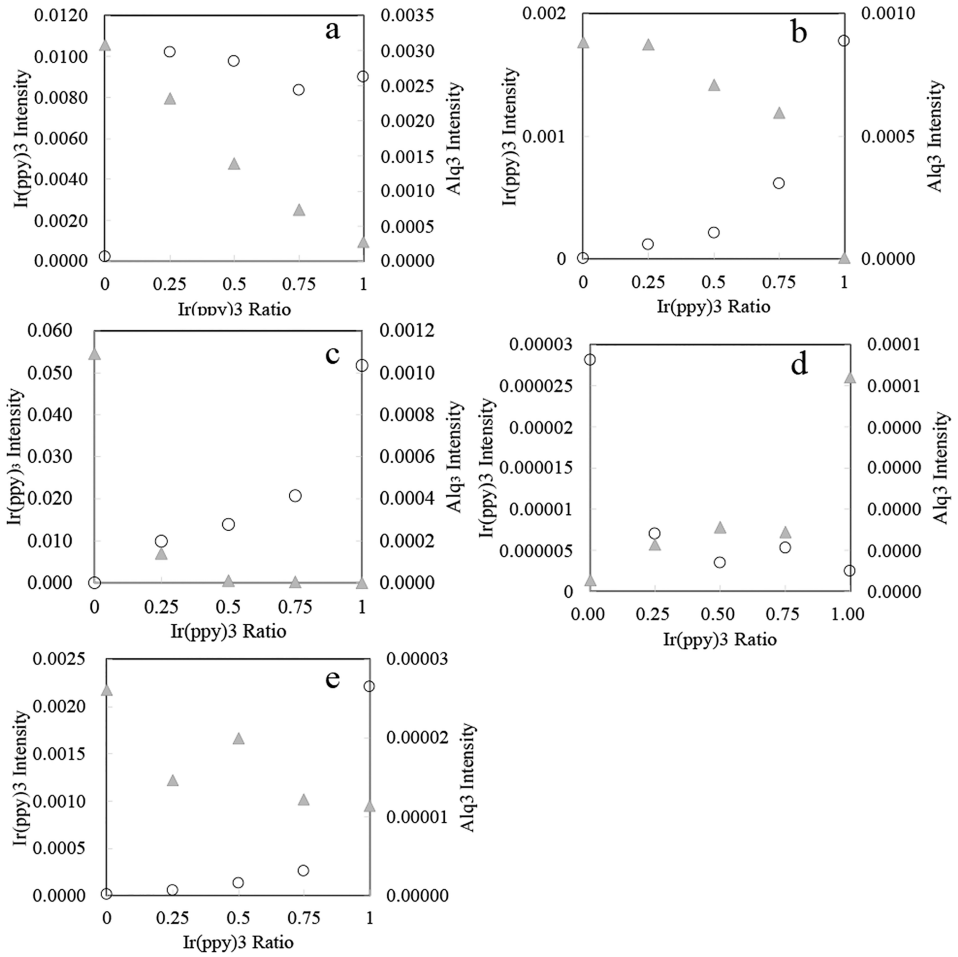

Figure 2. Calibration curves of ion intensities: (a) circle, m/z 655 for $Ir(ppy)_3$, and triangle, m/z 460 for Alq_3 obtained with TOF-SIMS using Bi_3^{2+}; (b) m/z 654 for $Ir(ppy)_3$ and 460 for Alq_3 obtained with J105 using H_2O cluster ions; (c) m/z = 655 for $Ir(ppy)_3$ and m/z = 459 for Alq_3 obtained with OrbiSIMS using Ar_{1400}^+; (d) m/z 655 for $Ir(ppy)_3$ and m/z 459 for Alq_3 obtained with LDI-TOF; (e) m/z 656 for $Ir(ppy)_3$ and m/z 460 for Alq_3 obtained with DINeC.

spectroscopic ellipsometry, demonstrating a film thickness of 35 nm for $Ir(ppy)_3$ to 43 nm for Alq_3 layers and compositions estimated from refractive index changes were estimated to be 22%, 48%, and 73% $Ir(ppy)_3$, in reasonable accord with the expected compositions.

Data Preparation for Machine Learning. Positive-ion results were evaluated in this study. The intensities of the peaks in the ToF-SIMS spectra of the monolayer samples were exported using the peak lists for SurfaceLab version 7.0.106074 and WinCadenceN version 1.11.1.24, which were prepared for

https://doi.org/10.1021/acs.analchem.3c03173
Anal. Chem. 2023, 95, 15078−15085

the previous VAMAS project TW2 A26 (Technical Working Area 2, Surface Chemical Analysis, A26). Details of the peak lists have been provided in a previous study.[29] There were 4230 peaks ranging from m/z 13 to 1214. The mass bin width is approximately 0.3 Da to distinguish inorganic and organic mass peaks. The intensities of the peaks were normalized to the total ion count. The normalized peak intensities were then used as descriptors (Table S2 of the Supporting Information). The peak intensities in the depth profile of the multilayer sample were exported by using the same peak list as the monolayer sample spectra. The intensity of each peak was normalized to the total ion count at each depth.

For the spectra of ToF-SIMS with a water cluster ion beam (J105), those of OrbiSIMS, those of DINeC, and those of LDI, the peak intensities in each spectrum were exported.

Simple ANN. A simple ANN was used for supervised learning analysis. A simple ANN composed of an input layer, one hidden layer, and an output layer (Figure 1) was developed by using Python 3. The hidden layer size was seven, and the transfer function was ReLU. Suppose there are s spectra with ν mass peaks (variables); the input matrix shape becomes $s \times \nu$. The reference monolayer samples with five ratios of $Ir(ppy)_3$ (0, 0.25, 0.5, 0.75, and 1) were used as the labels represented by one-hot encoding (1 or 0) for the ANN training. An example of the labels is presented in Table S3 in the Supporting Information. The output matrix shape was $s \times 5$ because there were five labels. The shape of the matrix of weights $W1$ for the input and the hidden layer was $\nu \times 7$, while that of the matrix of weights $W2$ for the hidden layer and the output layer was $s \times 5$. Therefore, the shape of the product of these weight matrices $W1$ and $W2$ was $\nu \times 5$.

The mass peak intensities of the monolayer samples were used as training data. In addition, some of the monolayer sample data sets or the multilayer sample data sets were used as test data. The simple ANN model was trained by minimizing the difference between the $Ir(ppy)_3$ ratio of each spectrum in the labels and the prediction using a simple ANN system (in the output).

Results. *Mass Spectra of OEL Mixed Samples.* Mass peaks related to the OEL molecules $Ir(ppy)_3$ and Alq_3 were searched in the mass spectra obtained by each method. The results showed that concentration dependency of the ion intensities specific to each material was not proportional to the material ratios in all results, ToF-SIMS with a Bi cluster ion beam, J105 (ToF-SIMS with a water cluster ion beam), OrbiSIMS, LDI-TOF, and DINeC as shown in Figure 2, because of the matrix effects, which are often observed in the mass spectra of multi component samples. The results obtained using J105 with a water cluster beam and those obtained using OrbiSIMS with an Ar cluster beam showed higher concentration dependence than the ToF-SIMS results although the calibration curves were not linear. The differences observed in OrbiSIMS are likely because of its much higher mass resolving power and therefore peaks in the OrbiSIMS spectra are rarely interfered by mass peaks from other molecules. In J105 with a water cluster ion beam, the water cluster ion beam produces molecular ions with higher sensitivity than other primary ion beams,[30] leading to the generation of molecule-related ions without the influence of interfering peaks. The LDI-TOF results showed high matrix effects as the intensities of the mixture samples were significantly suppressed or enhanced, regardless of the material ratios. In ToF-SIMS with a Bi cluster ion beam, the Alq_3 molecule peak showed a high concentration dependence, although the $Ir(ppy)_3$ molecule peak intensity was greatly influenced by matrix effects or interfering peaks from another material. DINeC is the softest ionization method among the ion beam analysis methods used in this study. The $Ir(ppy)_3$ molecular peak was strongly detected. Moreover, the concentration dependence of the $Ir(ppy)_3$ molecule peak in the DINeC spectra was high, although not linear. The Alq_3 molecule peak was not clearly observed by DINeC (within the noise level).

If appropriate mass peaks for quantitative analysis were found in the spectra, then calibration curves with a higher linearity could be obtained. Machine learning or multivariate analysis such as principal component analysis is generally useful for searching such peaks. However, peak searching processes are generally complicated. Therefore, an analysis method using the entire spectrum without peak selection was developed and compared among the different data sets as described in the next section.

Mass Spectrum Quantitative Analysis Using ANN. ToF-SIMS Spectrum Analysis. There were 30 ToF-SIMS spectra obtained using a Bi_3 ion beam. These spectra were converted into numerical data composed of 4230 mass peak intensities (variables) using the peak list prepared for the VAMAS project TW2 A26.[29] A simple ANN model was built by learning these 30 spectra (six spectra for each monolayer sample), and then the ratios of the depth profile data set of the multilayer sample were predicted. Although the number of the training spectrum data, 30, is generally small to build a model using machine learning, a model could be built because strictly prepared reference samples were employed and also because few types of ratios (0, 0.25, 0.5, 0.75, and 1) were investigated in this study. However, many more spectra will be necessary to predict the detailed ratio differences.

Typical prediction results for the monolayer sample spectra are listed in Table 1. The accuracy (ratio of the correctly predicted label number to the total label number in the test data set) was 0.96 (=144/150). Only three spectra (the correct $Ir(ppy)_3$ ratio of them was 0.5) were falsely predicted. Moreover, the range of the mistaken ratio was within 0.25. Some of the spectra of $Ir(ppy)_3$ ratios of 0.25, 0.50, or 0.75 were falsely predicted when the prediction using the simple ANN was repeated.

The matrix products of $W1$ and $W2$ indicate the mass peaks related to each label ($Ir(ppy)_3$ ratio). Mass peaks that greatly contribute to a label have high positive values for weights ($W1$ and $W2$) and mass peaks that make opposite high contributions to the same label have high negative values for the weights ($W1$ and $W2$). In other words, the multiplication of weight matrices between the input layer and the middle layer ($W1$) and that between the middle layer and the output layer ($W2$) provides positively high values for both cases, positively high elements (corresponding to the $Ir(ppy)_3$ ratio) in the weight matrices $W1$ and $W2$ and negatively high elements (corresponding to the Alq_3 ratio) in the weight matrices $W1$ and $W2$. Table 2 shows the important mass peaks to the $Ir(ppy)_3$ ratio 1 (pure $Ir(ppy)_3$), 0.5 (equally mixed sample), and 0 (pure Alq_3) labels, respectively, based on the multiplication of the weight matrices $W1$ and $W2$. The important peaks for pure $Ir(ppy)_3$, m/z 577.1 $[Ir(ppy)_3\text{-}C_5NH_4]^+$, and for pure Alq_3, m/z 442.1 $[Alq_3\text{-}OH]^+$, showed high concentration dependency, as Figure 3 shows. In addition, the top mass peak for label 0 (pure Alq_3), m/z 457.9 $[Ir(ppy)_3\text{-}IrH_4]^+$, in Table 1 showed a high concentration dependence on $Ir(ppy)_3$. This peak may work as an opposite factor for the Alq_3 ratio.

The example of hyperparameters and conditions of the simple ANN model in this study is shown in Table S4 of the Supporting

https://doi.org/10.1021/acs.analchem.3c03173
Anal. Chem. 2023, 95, 15078−15085

Table 1. ANN Prediction Results for ToF-SIMS Spectra (accuracy: 0.96)[a]

$Ir(ppy)_3$ ratio	1	0.75	0.50	0.25	0
1	1	0	0	0	0
1	1	0	0	0	0
1	1	0	0	0	0
1	1	0	0	0	0
1	1	0	0	0	0
1	1	0	0	0	0
0.75	0	1	0	0	0
0.75	0	1	0	0	0
0.75	0	1	0	0	0
0.75	0	1	0	0	0
0.75	0	1	0	0	0
0.75	0	1	0	0	0
0.50	0	0	(0)	(1)	0
0.50	0	0	(0)	(1)	0
0.50	0	0	1	0	0
0.50	0	(1)	(0)	0	0
0.50	0	0	1	0	0
0.50	0	0	1	0	0
0.25	0	0	0	1	0
0.25	0	0	0	1	0
0.25	0	0	0	1	0
0.25	0	0	0	1	0
0.25	0	0	0	1	0
0.25	0	0	0	1	0
0	0	0	0	0	1
0	0	0	0	0	1
0	0	0	0	0	1
0	0	0	0	0	1
0	0	0	0	0	1
0	0	0	0	0	1

[a]Falsely predicted results are within brackets.

Information. The hidden layer size can be larger to express an approximate model of more complex sample data. In addition, a transfer function can be replaced with other functions such as sigmoid and softmax functions if necessary.

J105, OrbiSIMS, LDI-TOF, and DINeC Spectra Analysis. The results of quantitative analysis using the simple ANN for the mass spectrum data sets of J105 (ToF-SIMS with a water cluster ion beam), OrbiSIMS (using an Ar cluster primary ion beam), LDI TOF-MS, and DINeC also showed a high accuracy (>0.9). The important mass peaks for predicting pure OEL samples ($Ir(ppy)_3$ or Alq_3), as indicated by the weights for the LDI data, include $[Ir(ppy)_3\text{-}H]^+$ and $[Alq_3\text{-}H]^+$ (Table S5 of the Supporting Information). Some of the items in the mass column in Table S5 have the same value because the mass bin widths of LDI data sets 1 and 2 were very narrow. In contrast, the important mass peaks for predicting DINeC, OrbiSIMS, and J105 include multimers such as trimers and tetramers (Table S6 of the Supporting Information); in particular, the important mass peaks for the DINeC data set are larger than those of the others. This is because the energy per molecule of DINeC clusters is much lower, approximately 0.8 eV/molecule, than that of Ar cluster ions or water cluster ions, leading to even softer desorption.[31] The mass bin width of J105 was also narrow (approximately 0.00025); therefore, the important mass peaks for the $Ir(ppy)_3$ ratio 1 suggested the same ion (Table S6c). The mass resolution of the OrbiSIMS data set was much higher than that of other data sets. Some of the important mass peaks in the OrbiSIMS data set (Table S6b) could be multiply charged ions, e.g., m/z 854.7199 is possibly a double charged ion $[(Alq_3)_4\text{-}C_9OH_3]^{2+}$; otherwise, appropriate formulas were not found for some of the mass peaks. Thus, the important mass peaks for representing a sample that are generally different, depending on the measurement condition, can be indicated by the simple ANN system. The mass peaks indicated by the simple ANN were useful for selecting specific peaks to the materials in the sample.

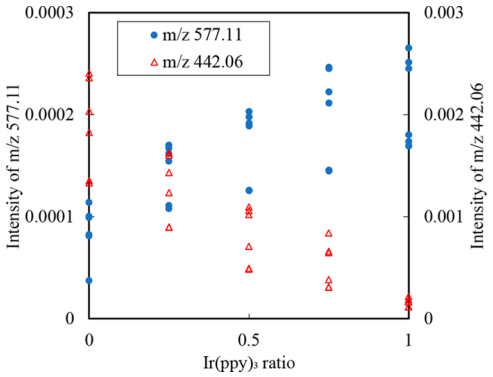

Figure 3. Concentration dependence of the mass peaks. The peaks m/z 577.11 and 442.06 were suggested by simple ANN quantitative analysis.

Multilayer Analysis and Matrix Effect Correction (ToF-SIMS Spectra). The multilayer sample containing pure layers and mixed layers, as shown in Figure 4a, was analyzed using SIMS and XPS. The relationships between the sputter time and the depth of the sample were different in ToF-SIMS and XPS results because the sputtering conditions were different. The depth profiles of the first four pure layers of the OEL materials

Table 2. Ten Most Important Mass Peaks with the Highest Ten Weight Products of *W*1 and *W*2 in the ANN for the ToF-SIMS Data of the Monolayers

*W*1*W*2 for $Ir(ppy)_3$ ratio 1	m/z	formula	*W*1*W*2 for $Ir(ppy)_3$ ratio 0	m/z	formula
9141	577.1	$[Ir(ppy)_3\text{-}C_5NH_4]^+$	9280	457.9	$[Ir(ppy)_3\text{-}IrH_4]^+$
8512	985.9	$[((Ir(ppy)_3)_2+H_6]^{2+}$	8884	442.1	$[Alq_3\text{-}OH]^+$
8407	514.1		8457	436.1	$[Alq_3+H\text{-}C_2]^+$
8352	939.5		8442	680.9	
8165	455.9		8078	603.1	
8097	531.1		8006	203.9	
7901	988.1		7721	907.9	
7880	972.9		7710	403.9	
7855	1027.1		7639	510.1	
7680	629.1		7623	699.9	

https://doi.org/10.1021/acs.analchem.3c03173
Anal. Chem. 2023, 95, 15078−15085

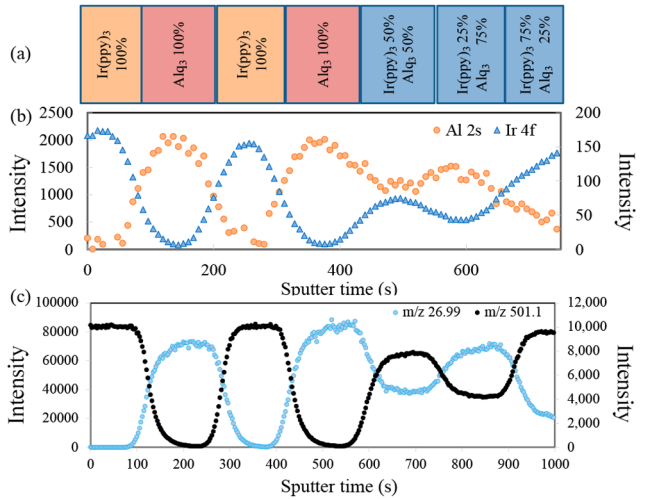

Figure 4. Analysis of the multilayer sample (a) by XPS (b) and ToF-SIMS (c). The mass peaks at m/z 26.99 and 501.1 are related to Alq_3 and $Ir(ppy)_3$, respectively.

obtained using ToF-SIMS were consistent with the XPS profiles. The XPS depth profiles indicated that the first four pure layers of $Ir(ppy)_3$ and Alq_3 and the mixed layers comprising $Ir(ppy)_3$ and Alq_3 (0.5:0.5 and 0.25:0.75) were appropriately preserved. However, in the deepest $Ir(ppy)_3$ and Alq_3 mixed layer (0.75:0.25), the molecules might have been mixed or diffused. The ToF-SIMS depth profiles of the mixed layers differed from those of the sample mixture ratios because of matrix effects, although the XPS profiles were consistent with the OEL material ratios in the sample. In addition, the layer thickness may not be sufficient to obtain clear depth profiles because the thickness of each layer was 50 nm.

Several methods have been proposed for matrix-effect correction.[3−12] This study employed one of the simplest methods based on RSF. The ratio of a material in the mixture was calculated using the following equation:

$$C_{Ai} = \frac{I_{Ai}}{I_{Ai} + \mathrm{RSF} I_B}$$

where C_{Ai} is the calculated ratio of material A in a ratio i sample, I_{Ai} is the intensity of a peak from A in the ratio i sample, I_B is the intensity of a peak from material B in a ratio $1-i$ sample, and RSF is the ratio of the relative sensitivities of B and A.

For the matrix-effect correction, the mass peaks at m/z 501.1 ($Ir(ppy)_3$-$C_6H_4C_5NH_4^+$) and 26.99 (Al^+) from $Ir(ppy)_3$ and Alq_3, respectively, were used because their intensities in the pure materials (ratio 1) were high enough compared to the intensities in the samples with a ratio 0. The correlation coefficients for the peaks at m/z 501.1 and 26.99 were 0.922 and 0.960, respectively, both of which became 0.999 after the matrix-effect correction (Figure 5). Moreover, the matrix-effect correction result was also used to calculate the OEL material ratios of the multilayer sample (Figure 6).

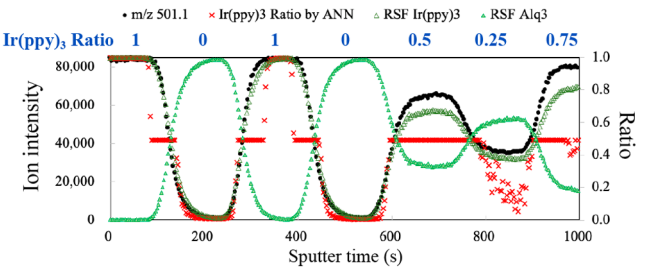

Figure 6. Depth profiles of the multilayer sample. Closed circle: mass peak m/z 501 intensity related to $Ir(ppy)_3$ ratio, ×: $Ir(ppy)_3$ ratio predicted by the simple ANN, open triangle: $Ir(ppy)_3$ ratio predicted by matrix-effect correction based on RSF, and closed triangle: Alq_3 ratio predicted by matrix-effect correction based on RSF.

The ToF-SIMS depth profiles of the multilayer sample were predicted using the simple ANN. To build this simple ANN model, the ratios of $Ir(ppy)_3$ were used as the labels, and the ToF-SIMS spectra of the monolayer samples (the same 30 ToF-SIMS spectra obtained using a Bi_3 ion beam as the spectra used in the ToF-SIMS spectrum analysis section) were used as the descriptors. In addition, the ToF-SIMS spectra of the Si substrate after removing the OEL layer were also added to the data set to provide the ratio 0 sample data. There are two types of the ratio 0 (without $Ir(ppy)_3$) samples: one is the pure Alq_3 sample, and the other one contains neither $Ir(ppy)_3$ nor Alq_3.

Figure 6 shows the OEL material ratios predicted using the matrix-effect correction method and the simple ANN. The $Ir(ppy)_3$ ratios of the pure layers and the layer containing 50% $Ir(ppy)_3$ were correctly predicted using the simple ANN. The ratio at each sputter time (depth) was calculated by multiplying the label class ($Ir(ppy)_3$ ratios) and the ANN prediction value of the label, as shown in Table S8 of the Supporting Information.

The ratios predicted by the simple ANN were roughly correct in terms of the interfaces between the pure layers. However, the interface profiles obtained by both methods (the simple ANN and matrix-effect correction) were different from the XPS profiles. In the middle of the interfaces between the pure layers, several depth points were predicted as $Ir(ppy)_3$ ratio 0.5 by the

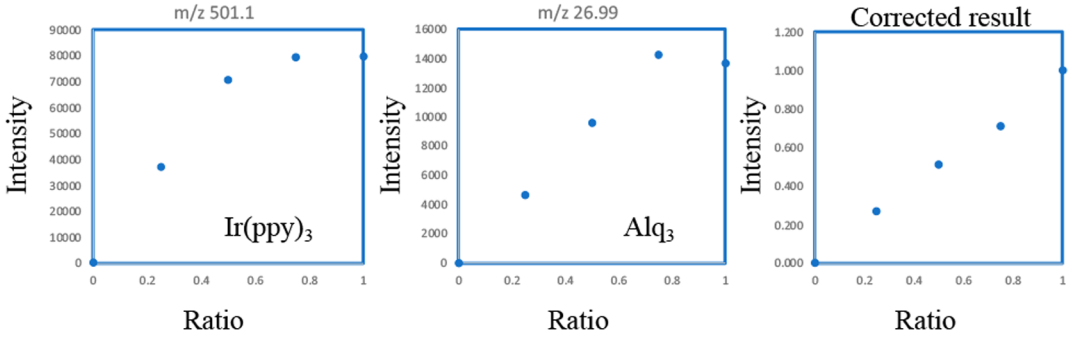

Figure 5. Calibration curves before and after the matrix effect correction by the relative sensitivity factor (RSF).

https://doi.org/10.1021/acs.analchem.3c03173
Anal. Chem. 2023, 95, 15078−15085

simple ANN, probably because the reference sample types, i.e., $Ir(ppy)_3$ ratios 0, 0.25, 0.5, 0.75, and 1, were not sufficient. More reference samples with a variety of ratios close to 0.5 might be needed to predict ratios that are slightly different from those of approximately 0.5. In addition, a larger number of spectra may also be necessary to build a more effective model to express matrix effects. Moreover, peak selection should be improved for a more precise prediction regarding the matrix-effect correction.

In the simple ANN model for multilayer sample prediction, the important mass peaks for each $Ir(ppy)_3$ ratio were similar. Table 3 shows the important mass peaks related to $Ir(ppy)_3$ ratios of 1 and 0 samples. The important mass peaks related to all-ratio samples are shown in Table S7. The important peaks correspond to ions related to $Ir(ppy)_3$ and Alq_3; some of these peaks are larger than molecular ions. The important mass peaks (Table S7) include the peaks at m/z 26.99 (Al^+), because the matrix effects of Alq_3 were lower than those of $Ir(ppy)_3$, as shown in Figure 4c. In addition, although the smallest ion (m/z 49.01) showed low $Ir(ppy)_3$ ratio dependence, it was sensitive to the interface between the Si substrate and the OEL (Figure S3). However, this peak was not indicated by the simple ANN when only the OEL monolayer sample data were analyzed (Table 2).

Table 3. Ten Shows the Most Important Mass Peaks with the Highest Weight Products of *W*1 and *W*2 in the ANN for the Multilayer Sample Prediction[a]

$Ir(ppy)_3$ ratio 1	m/z	formula	$Ir(ppy)_3$ ratio 0	m/z
73.99	49.01	$C_4H^+/SiOH_5^+$	74.37	49.01
72.21	26.99	Al^+	72.02	26.99
71.72	475.08	$[Ir(ppy)_3\text{-}Ir+CH]^+$	71.53	475.08
71.45	739.13	$[Ir(ppy)_3+C_5NH_6]^+$	71.23	739.13
70.94	288.95	$[Alq_3\text{-}\ C_9NOH_6\text{–}CN]^+$	70.63	288.95
69.00	777.98	Related to Alq_3	69.05	777.98
66.83	517.44	$[Ir(ppy)_3\text{-}Ir+C_3NH_5]^+$	66.94	1053.0
66.75	1053.0	Related to $Ir(ppy)_3$	66.89	517.44
66.27	328.09	Related to Alq_3	66.43	328.09
66.24	99.98	Related to Alq_3	66.26	99.98

[a]Mass bin width is approximately 0.3 Da.

The depth profiles of these mass peaks represented in Figure S3 in the Supporting Information. Peaks m/z 328.09 and 288.95 were highly dependent on the Alq_3 ratio, while peaks m/z 517.44 and 475.08 were highly dependent on the $Ir(ppy)_3$ ratio. Thus, the simple ANN indicated not only the material ratios in the unknown samples but also the mass peaks related to each molecule in the sample. This is of practical importance for the analysis of mass spectrum and mass image data because the information on important ions specific to each material in a sample is crucial for the spectrum interpretation and mass imaging. Moreover, selecting the appropriate ions for such an analysis is one of the most complicated issues in the analysis of complex samples. Thus, this study indicates that the simple ANN method is particularly useful for the initial analysis of complex samples containing unknown materials.

CONCLUSIONS

Mass spectra of the binary mixtures of the OEL molecules, $Ir(ppy)_3$ and Alq_3, were analyzed using a simple ANN system for both quantitative and qualitative analyses. By learning the reference samples (the mixtures of five ratios), the material ratios of unknown samples, whose ratios are naturally unknown, and the interfaces between layers with different materials or mixtures of different material ratios were determined using a simple ANN system. Moreover, the matrix product of the weights in the simple ANN model provides information on the important mass peaks related to the materials in the samples although finding such mass peaks related to each material in a complex sample is generally difficult. The simple ANN may be useful for qualitative analysis and the identification of strategies to quantify the sample, and hence is particularly useful for the initial analysis of complex samples containing unknown materials.

ASSOCIATED CONTENT

Supporting Information

The Supporting Information is available free of charge at https://pubs.acs.org/doi/10.1021/acs.analchem.3c03173.

Samples in terms of strains and cultures are described. Figure S1: Schematic of the samples; Figure S2: Simple artificial neural network (ANN); Figure S3: Depth profiles of the ions important to the ANN model for the multilayer sample; Figure S4: The ANN prediction for all layers; Figure S5: The XPS depth profiles of all layers; Table S1: ToF-SIMS measurement condition examples; Table S2: Example of the descriptors; Table S3: Example of the labels; Table S4: The example of main hyperparameters and conditions for the simple ANN; Table S5(a): *W*1*W*2 for LDI data set 1; Table S5(b): *W*1*W*2 for LDI data set 2; Table S6(a): *W*1*W*2 for DINeC data set; Table S6(b): *W*1*W*2 for OrbiSIMS data set; Table S6(c): *W*1*W*2 for J105 data set; Table S7: Ten most important mass peaks with highest weight products of *W*1 and *W*2 in the ANN for the multilayer sample prediction; Table S8: Example of the calculation for the ANN prediction ratios of the multilayer sample (PDF)

AUTHOR INFORMATION

Corresponding Author

Satoka Aoyagi − *Faculty of Science and Technology, Seikei University, Musashino, Tokyo 180-8633, Japan;* orcid.org/0000-0001-7100-7179; Email: aoyagi@st.seikei.ac.jp

Authors

David J. H. Cant − *National Physical Laboratory, Teddington, Middlesex TW11 0LW, United Kingdom;* orcid.org/0000-0002-4247-5739

Michael Dürr − *Institute of Applied Physics and Center for Materials Research, Justus Liebig University Giessen, 35394 Giessen, Germany;* orcid.org/0000-0002-4676-8715

Anya Eyres − *National Physical Laboratory, Teddington, Middlesex TW11 0LW, United Kingdom*

Sarah Fearn − *Department of Materials, Imperial College London, London SW7 2AZ, United Kingdom*

Ian S. Gilmore − *National Physical Laboratory, Teddington, Middlesex TW11 0LW, United Kingdom;* orcid.org/0000-0002-0981-2318

Shin-ichi Iida − *ULVAC-PHI, Inc., Chigasaki, Kanagawa 253-8522, Japan*

Reiko Ikeda − *Analytical Science Research Laboratory, Kao Corp., Wakayama-shi, Wakayama 640-8580, Japan*

Kazutaka Ishikawa − *Analytical Science Research Laboratory, Kao Corp., Wakayama-shi, Wakayama 640-8580, Japan*

Matija Lagator − *Photon Science Institute, Department of Chemistry, University of Manchester, Manchester M13 9PL, United Kingdom*
Nicholas Lockyer − *Photon Science Institute, Department of Chemistry, University of Manchester, Manchester M13 9PL, United Kingdom;* orcid.org/0000-0002-9674-9395
Philip Keller − *Institute of Applied Physics and Center for Materials Research, Justus Liebig University Giessen, 35394 Giessen, Germany*
Kazuhiro Matsuda − *Surface Science Laboratories, Toray Research Center, Inc., Otsu, Shiga 520-8567, Japan*
Yohei Murayama − *Specialty Chemicals Development Center, Peripheral Products Operations, Canon Inc., Susono, Shizuoka 410-1196, Japan*
Masayuki Okamoto − *Analytical Science Research Laboratory, Kao Corp., Wakayama-shi, Wakayama 640-8580, Japan*
Benjamen P. Reed − *National Physical Laboratory, Teddington, Middlesex TW11 0LW, United Kingdom*
Alexander G. Shard − *National Physical Laboratory, Teddington, Middlesex TW11 0LW, United Kingdom;* orcid.org/0000-0002-8931-5740
Akio Takano − *Toyama Co., Ltd., Yamakita-machi, Ashigarakami-gun Kanagawa 258-0112, Japan*
Gustavo F. Trindade − *National Physical Laboratory, Teddington, Middlesex TW11 0LW, United Kingdom;* orcid.org/0000-0001-6998-814X
Jean-Luc Vorng − *National Physical Laboratory, Teddington, Middlesex TW11 0LW, United Kingdom;* orcid.org/0000-0001-9627-1574

Complete contact information is available at: https://pubs.acs.org/10.1021/acs.analchem.3c03173

Author Contributions

All the authors approved the final version of the manuscript. The manuscript was written with contributions from all authors. A.E., G.T.F., and I.S.G. provided the OrbiSIMS data, J.L.V., S.F., R.I., M.O., Y.M., S.I., and K.M. provided ToF-SIMS data, M.L. and N.L. provided J105 data, K.I., M.O., and Y.M. provided LDI data, P.K. and M.D. provided DINeC data, D.J.H.C., B.P.R., and A.G.S. provided XPS data, A.T. and S.A. prepared the samples, and S.A. analyzed whole data by using machine learning methods.

Notes

The authors declare no competing financial interest.

■ ACKNOWLEDGMENTS

This work was partly supported by JSPS KAKENHI, Grant No. 17K05908, Japan. DC, ACSE, ISG, BPR, AGS, GFT, and JLV were supported by the U.K. Government's Department for Science, Innovation and Technology (DSIT).

■ REFERENCES

(1) Busch, K. L.; Hsu, B. H.; Xie, Y. X.; Cooks, R. G. *Anal. Chem.* **1983**, *55*, 1157−1160.
(2) GaO, Y. *J. Appl. Phys.* **1988**, *64*, 3760.
(3) Shard, A. G.; Havelund, R.; Spencer, S. J.; et al. *J. Phys. Chem. B* **2015**, *119*, 10784−10797.
(4) Shard, A. G.; Rafati, A.; Ogaki, R.; Lee, J. L.; Hutton, S.; Mishra, G.; Davies, M. C.; Alexander, M. R. *J. Phys. Chem. B* **2009**, *113*, 11574−11582.
(5) Shard, A. G.; Spencer, S. J.; Smith, S. A.; Havelund, R.; Gilmore, I. S. *Int. J. Mass Spectrom.* **2015**, *377*, 599−609.
(6) Seah, M. P.; Havelund, R.; Gilmore, I. S. *J. Phys. Chem. C* **2016**, *120*, 26328−26335.
(7) Takahashi, K.; Aoyagi, S.; Kawashima, T. *Surf. Interface Anal.* **2017**, *49*, 721−727.
(8) Breuer, L.; Popczun, N. J.; Wucher, A.; Winograd, N. *J. Phys. Chem. C* **2017**, *121*, 19705−19715.
(9) Seah, M. P.; Shard, A. G. *Appl. Surf. Sci.* **2018**, *439*, 605−611.
(10) Havelund, R.; Seah, M. P.; Gilmore, I. S. *Surf. Interface Anal.* **2019**, *51*, 1332−1341.
(11) Seah, M. P.; Havelund, R.; Spencer, S. J.; Gilmore, I. S. *J. Am. Soc. Mass Spectrom.* **2019**, *30*, 309−320.
(12) Shard, A. G.; Miisho, A.; Vorng, J.-L.; Havelund, R.; Gilmore, I. S.; Aoyagi, S. *Surf. Interface Anal.* **2022**, *54*, 363−373.
(13) Borisov, R. S.; Polovkov, N. Y.; Zhilyaev, D. I.; Zaikin, V. G. *Rapid Commun. Mass Spectrom.* **2013**, *27*, 333−338.
(14) Gilmore, I. S. *J. Vac. Sci. Technol. A* **2013**, *31*, 050819.
(15) Vickerman, J. C.; Briggs, D. *ToF-SIMS: Materials Analysis by Mass Spectrometry*, 2nd ed.; I M Publications LLP: Chichester, U.K., 2013.
(16) Kawashima, T.; Aoki, T.; Taniike, Y.; Aoyagi, S. *Biointerphases* **2020**, *15*, 031013.
(17) Matsuda, K.; Aoyagi, S. *Biointerphases.* **2020**, *15*, 021013.
(18) Matsuda, K.; Aoyagi, S. *Anal. Bioanal. Chem.* **2022**, *414*, 1177−1186.
(19) Aoyagi, S.; Matsuda, K. *Mass Spectrom.* **2023**, *37*, No. e9445.
(20) Lee, J. L. S.; Gilmore, I. S.; Fletcher, I. W.; Seah, M. P. *Surf. Interface Anal.* **2009**, *41*, 653−665.
(21) Yokoyama, Y.; Kawashima, T.; Ohkawa, M.; Iwai, H.; Aoyagi, S. *Surf. Interface Anal.* **2015**, *47*, 439−446.
(22) Takayasu, S.; Suzuki, T.; Shinozaki, K. *J. Phys. Chem. B* **2013**, *117*, 9449−9456.
(23) Wang, M.-H.; Konya, T.; Yahata, M.; Sawada, Y.; Kishi, A.; Uchida, T.; Lei, H.; Hoshi, Y.; Sun, L.-X. *J. Therm. Anal. Calorim.* **2010**, *99*, 117−122.
(24) Fletcher, J. S.; Rabbani, S.; Henderson, A.; Blenkinsopp, P.; Thompson, S. P.; Lockyer, N. P.; Vickerman, J. C. *Anal. Chem.* **2008**, *80* (23), 9058−9064.
(25) Passarelli, M. K.; Pirkl, A.; Moellers, R.; Grinfeld, D.; Kollmer, F.; Havelund, R.; Newman, C. F.; Marshall, P. S.; Arlinghaus, H.; Alexander, M. R.; West, A.; Horning, S.; Niehuis, E.; Makarov, A.; Dollery, C. T.; Gilmore, I. S. *Nat. Methods* **2017**, *14*, 1175−1183.
(26) Matjacic, L.; Seah, M. P.; Trindade, G. F.; Pirkl, A.; Havelund, R.; Vorng, J.-L.; Niehuis, E.; Gilmore, I. S. *Surf. Interface Anal.* **2022**, *54*, 331−340.
(27) Gebhardt, C. R.; Tomsic, A.; Schröder, H.; Dürr, M.; Kompa, K.-L. *Angew. Chem., Int. Ed.* **2009**, *48*, 4162−4165.
(28) Baur, M.; Gebhardt, C. R.; Dürr, M. *Rapid Commun. Mass Spectrom.* **2014**, *28*, 290−296.
(29) Aoyagi, S.; Fujiwara, Y.; Takano, A.; Vorng, J. L.; Gilmore, I. S.; Wang, Y. C.; Tallarek, E.; Hagenhoff, B.; Iida, S. I.; Luch, A.; Jungnickel, H.; Lang, Y.; Shon, H. K.; Lee, T. G.; Li, Z.; Matsuda, K.; Mihara, I.; Miisho, A.; Murayama, Y.; Nagatomi, T.; Ikeda, R.; Okamoto, M.; Saiga, K.; Tsuchiya, T.; Uemura, S. *Anal. Chem.* **2021**, *93*, 4191−4197.
(30) Sheraz neé Rabbani, S.; Berrueta Razo, I.; Kohn, T.; Lockyer, N. P.; Vickerman, J. C. *Anal. Chem.* **2015**, *87*, 2367−2374.
(31) Portz, A.; Bomhardt, K.; Rohnke, M.; Schneider, P.; Asperger, A.; Gebhardt, C. R.; Dürr, M. *Biointerphases* **2020**, *15*, 021001.